RSC Advances

PAPER

View Article Online
View Journal | View Issue

Cite this: *RSC Adv.*, 2026, **16**, 24595

Predictive modelling of multi-functional properties in XCuSO (X = Nd, Pr) oxychalcogenides *via* an *ab initio* approach

Safia Abdullah R. Alharbi[a] and Muhammad Salman Khan *[b]

This first-principles GGA+U study thoroughly examines the electronic, optical, elastic, and thermoelectric nature of NdCuSO and PrCuSO rare-earth oxychalcogenides. Structural optimizations confirm thermodynamic stability having negative formation energy values of −3.24 eV f.u.$^{-1}$ and −3.46 eV f.u.$^{-1}$, and cohesive energies of −4.21 eV f.u.$^{-1}$ and −4.63 eV f.u.$^{-1}$ for NdCuSO and PrCuSO, respectively. Electronic band structures demonstrate intrinsic half-metallicity, with the spin-up case being metallic with the Fermi level crossing the conduction band, while the spin-down case shows semiconductor nature with energy gap values of ∼1.2 eV (NdCuSO) and ∼1.0 eV (PrCuSO), leading to approximately 100% spin polarization. The density of states study revealed dominating Cu-3d states at the valence band edge, and Nd/Pr-4f states ranging from 2–4 eV in the conduction band, and deep O-2p/S-3p bonding states, confirming significant orbital-resolved hybridization and magnetic asymmetry. Elastic constants satisfy the criteria of mechanical stability, with medium-stiffness (B = 87.8–91.7 GPa, Y = 118–126 GPa), ductile behaviour (B/G 1.9 with positive Cauchy pressure), and high elastic anisotropy (A = 0.91–0.95). Optical spectra were displayed showing high static dielectric constants, strong interband transitions at less than 2 eV, low visible reflectivity (less than 0.3), noticeable UV absorption at 7–12 eV, and plasmon resonances at 15–18 eV, showing their suitability for the optoelectronics technologies and UV-photonic. Between 300–500 K, the conduction of n-type was predicted because of the decrease in Seebeck coefficients between −6.5 to −9.2 μV K^{-1} in NdCuSO, and −7.2 to −10.3 μV K^{-1} in PrCuSO material. The ZT rises to 0.48 and 0.41, driven by greater electrical conductivity along with lower thermal conductivity in NdCuSO material.

Received 26th January 2026
Accepted 4th May 2026

DOI: 10.1039/d6ra00700g

rsc.li/rsc-advances

1. Introduction

The primary issue with modern thermoelectric power generators is an oversupply of other green energy resources that convert heat into energy and *vice versa*.[1] The difficulty stimulates us to consider materials capable of capturing some of the unused heat energy and converting it to electricity.[2] Oxychalcogenides, such as BiCuXO (X = S, Se), possess a layered structure of the ZrCuSiAs type that was discovered by Johnson *et al.* in 1974,[3] and have surfaced as Te systems capable of having inherently lower lattice thermal conductivity and a substantial Seebeck coefficient.[4] The oxychalcogenides have a tetragonal crystal structure of RMChO (1111) stoichiometry, with a space group ($P4/nmm$) comprising the rare-earth element, or Bi, along with the Cu, Ag, and chalcogenides, with M = Ag, as transparent conductors.[5] According to Jing Li *et al.*[6] and Yanling Pei *et al.*,[7] the greater figure of merit for BiCuSeO oxychalcogenide is primarily because of a remarkably lower lattice thermal conductivity of 0.2 W m^{-1} K^{-1} at high temperatures. Pratik Shukla *et al.*[8] investigated the structural and transport features of oxychalcogenides, finding the maximum figure of merit. In addition, Zou *et al.*[9] discovered the Seebeck coefficient of greater power factor that was 177 μV K^{-1} and 182 μV K^{-1} for BiCuSeO and BiCuSO oxychalcogenides at 700 K. Yang *et al.*[10] anticipate that the highest values of figure of merit (ZT) for BiCuSeO are 0.91 and 1.2 for the p and n-type doping of 3.2 × 10^{20} and 4.6 × 10^{19} cm^{-3}, respectively. Fan *et al.*[11] were the first to compute the electronic and phonon transport parameters of the BiCuSeO material using a first-principles calculation. R. Viennois *et al.*[12] investigated the lattice dynamics of BiCuChO (Ch = Se, S) materials experimentally and used density functional theory (DFPT) simulations to demonstrate the substantial anharmonic nature of BiCuSeO. Otherwise, these materials were also of special significance in improving optoelectronic and photovoltaic appliances. O. Arbouche *et al.*[13] analyzed the tetragonal structure of BiCuSO and BiCuSeO and investigated the physical properties of these materials. The two materials are ductile and sound. It was perceived that the optical properties of the oxychalcogenides are

[a]*Department of Physics, College of Science, Imam Mohammad Ibn Saud Islamic University (IMSIU), Riyadh, 11623, Saudi Arabia*
[b]*Department of Physics, Abdul Wali Khan University, Mardan, 23200, Pakistan. E-mail: salmankhan73030@gmail.com*

effective materials in the application of solar cells. BiCuSO and BiCuSeO materials have greater PF with n-type doping as compared with p-type doping at 1200 K.[13] It was stated that the Bi^{3+} ion at the Ln position in BiCuSeO materials shows better thermoelectric features and good stability.[14,15] In undoped BiCuSeO, orbital contributions to CBM are dominated by Bi 6p, with the consequence that the band gap is greatly reduced to 0.8 eV. Generally, RCuO (R = rare-earth) are wide gap p-type semiconductors (E_g = 3 eV), in which the VBM and CBM are close to the Γ point of the BZ. VBM in both RCuSeO and BiCuSeO comprises of hybridized Cu-3d and Se-4p orbitals.[16] Another p-type semiconductor is the BiCuSeO with a narrow band gap of about 0.8 eV. The presence of Bi-6p orbitals at the bottommost conduction band region induces evolution of the band structure. BiCuSeO oxyselenides have gained much interest and have been widely studied as good thermoelectric material families free of Pb because of their intrinsically low heat conductivity and relatively high Seebeck coefficient. Dually doped BiCuSeO at 923 K has an excellent performance in thermoelectric, with a figure of merit of 1.5 in the form of a dimensionless number.[17,18] To improve BiCuSeO, *ZT* with low κ, one way is to optimize charge carrier concentration. This can be done by partially substituting Bi^{3+} with divalent or monovalent ions to induce additional holes.[19] Optimizing carrier concentration to improve power factor ($\alpha^2\sigma$) is problematic due to the intrinsic coupling between the electrical conductivity and Seebeck coefficient. Oxychalcogenides of the rare-earths have attracted attention since the middle of the twentieth century, when the Ln_2O_2S was a phosphor in cathode ray tubes. The recent revival of oxychalcogenides may be owed to recent methods of computationally-tooled materials screening, as a number of recent articles have pointed out the effectiveness of oxychalcogenides in a wide range of applications, including p-type transparent semiconductors,[20] thermoelectrics,[21] and solid-state electrolytes.[22]

A novel exploration has studied the recent progress in synthetic methods to regulate chemical and physical properties through combining anions.[23] The oxysulfide family, BiCuOCh, CuOCh replaced here by S, Se or Te, was first discovered in 1994 by Kusainova *et al.*[24] The corresponding chemicals crystallize in the tetragonal *P*4/*nmm* space group. It is structured in layers of $(Bi_2O_2)_2$ and $(Cu_2Ch_2)_2$. The thermoelectric properties of BiCuOCh phases have been highly studied because of their low thermal conductivity and high electronic conductivity properties.[25,26] In fact, they have intrinsically low band gaps (0.4 eV for BiCuOTe and 1.1 eV for BiCuOS) and degenerated p-type semiconductors.[27] It seems that the copper vacancies in the QCuOCh system (Q = Bi or La) are thermodynamically favourable because their formation energy is low.[28] The structure is seemingly intrinsically generating copper vacancies in BiCuOS, as indicated in a high-resolution transmission electron microscopy (HR-TEM) study. The real composition of our powders, which we have observed, of $BiCu_{10.06}OS$, is verified by neutron diffraction investigation.[29] Le Bahers *et al.*[30] recently discovered BiCuOS to be a capable compound in heterojunction solar cells. Simulations of band structures indicate that this compound satisfies all the characteristics of an absorber (p-type) layer, such as a band gap of 1.1 eV to 1.4 eV.[31] But the carrier concentration in the structure was produced by each copper vacancy, which is determined to be excessive (optimal range of 10^{15} to 10^{17} cm^{-3}), which reduces the diffusion length of the electron holes generated by photochemical means. Even though the oxygen and chalcogen anions normally have a coordinating effect on each cation in oxychalcogenides, the case with LnCuOCh oxychalcogenides is different because of the layered crystalline structure; the chalcogen anions are the only coordinating anions of the copper cation, which affects the abnormal reduction of unit cell volume in the monophase. Numerous studies were carried out on oxychalcogenides. The oxyselenides, $La_{1-x}Sr_xCuOSe$, had degenerate p-type electrical conductivity due to the addition of Sr.[32] Including S in LaCuOS caused high optical transmission with ≥70% in visible and closer infrared regions, a band gap of approximately 3.1 eV, and with positive Seebeck coefficient values, indicating p-type conducting nature.[33] K. Ueda *et al.*[34] discovered that replacing metal atoms with chalcogens in LaMChO compounds (M = Cu, Ag; Ch = S, Se) resulted in anisotropic distortion of the crystal lattice and a decrease in the band gap of the semiconductors, with only weak direct interband transitions resulting from the combined ionic and covalent characteristics of the bonding. The latest progress in the density functional theory (DFT) has facilitated a thorough study of complicated materials, especially Cu-based chalcogenide alloys, in which structural, thermodynamic, mechanical, electronic, and optical properties have been studied systematically with the goal of realizing their multifunctional abilities.[35] Similarly, the first-principles research on quaternary type materials has also provided useful insights into their structural stability as well as electronic, mechanical, and optical properties, and their appropriateness in hydrogen storage applications.[36] Besides this, DFT-based approaches have been widely used to study the optoelectronic, photovoltaic, and mechanical characteristics of a wide range of oxide materials, which provide prospective information about energy-related technology.[37] In addition to these, interesting findings have been made by the *ab initio* simulations proving their applicability to multi-level phase-change memory devices.[38] Moreover, the experiment of novel SiGe allotropes with direct band gaps and improved electronic and optical performance proves the significance of first-principles techniques in the development of new functional materials.[39] Collectively, these studies underscore the flexibility and assurance of DFT in forecasting and designing material features to suit the next generation of technological uses. This is the first full first-principles examination of the rare-earth oxychalcogenides NdCuSO and PrCuSO, broadening the family by incorporating lighter lanthanides with unique electrical and transport properties. By incorporating structural stability analysis with spin-resolved electronic, elastic, optical, and thermoelectric properties, this research develops clear structure–property relationships and reveals half-metallicity, mechanical ductility, strong UV-visible optical activity, and have n-type thermoelectric nature. The results show that rare-earth substitution is a great approach to tune multifunctional reactions, providing predictive advice to

develop next-generation spintronic, optoelectronic, and energy-conversion materials.

2. Computational method

The GGA+U approach is an extension of the traditional Density Functional Theory (DFT) framework that incorporates an on-site Coulomb correction U that describes the strong electronic interactions present in the localized d or f states.[40] The GGA+U formalism defines total energy as the sum of GGA energy and a Hubbard correction component that penalizes fractional occupancies of localized states, restoring normal electronic localization and magnetic behaviour.[41] The GGA+U method improves the description of electronic, magnetic, optical, and thermoelectric properties by including two parameters: the on-site Coulomb interaction U, which measures the strength of repulsion among localized electrons, and the exchange parameter J, which accounts for intra-atomic exchange interactions. The effective Hubbard term, $U_{\text{eff}} = U - J$, is commonly used to alter the potential of localized orbitals without double-counting electron interactions, which are already accounted for in the GGA. The U_{eff} values have been assigned as 6.0 eV for Nd-4f, 5.5 eV for Pr-4f, and 4.5 eV for Cu-3d orbitals, which are consistent with previous studies for rare-earth and transition-metal systems. Brillouin zone integrations were carried out with an $8 \times 8 \times 6$ Monkhorst–Pack k-point mesh. These carefully determined parameters ensure that structural, electronic, and related properties may be predicted with confidence and reproducibility. Geometry optimization is done until Hellmann–Feynman forces on each atom are less than 0.01 eV Å^{-1}, and total energy is within 10^{-6} eV per atom. The energy cutoff of plane-wave $R \times K_{\max} = 8$ was used. Spin-polarized calculations are necessary to estimate the magnetic moments associated with localized f or d electrons. The GGA+U correction shifts occupied and unoccupied states in the density of states (DOS), increases the band gap, and produces better experimental electronic and optical spectra than ordinary GGA. Furthermore, GGA+U improve the prediction of mechanical stability and thermoelectric features since exact electronic band topologies have a direct impact on transport coefficients.

3. Results and discussions

3.1 Structural properties

NdCuSO forms in the tetragonal *I4mm* space group (see Fig. 1). The alternating CuS and NdO sheets are positioned in the (0, 0, 1) direction. The CuS layer coordinates each Cu^+ ion with four identical S^{2-} ions, producing CuS_4 tetrahedra with shared edges and corners. Cu–S bond lengths are 2.42 Å. Each S^{2-} ion forms a four-coordinate setting by connecting to four identical Cu^+ ions. The NdO layer consists of four-coordinate Nd^{3+} ions bound to four comparable O^{2-} ions. Four Nd^{3+} ions coordinate each O^{2-} ion, producing Ond_4 tetrahedra with shared corners and edges. PrCuSO crystallizes in the tetragonal *I4mm* space group and alternating CuS and PrO sheets arranged in the (0, 0, 1) direction. In the CuS layer, Cu^+ ions bind with four S^{2-} ions to create CuS_4 tetrahedra that share edges and corners. Cu–S bond lengths are 2.42 Å. S^{2-} ions are four-coordinated by comparable Cu^+ ions. The PrO layer consists of Pr^{3+} ions coupled to four identical O^{2-} ions in a tetrahedral arrangement. The Pr–O bond lengths are 2.35 Å. The O^{2-} ion attaches to four comparable Pr^{3+} ions, making Opr_4 tetrahedra with common edges and corners. Fig. 4(a) and (b) depicts the energy–volume optimization curves for the NdCuSO and PrCuSO rare-earth oxychalcogenides, which are significant for determining their equilibrium structural properties and thermodynamic stability. Both curves show the predicted parabolic or U-shaped tendency of Birch–Murnaghan-type behaviour, with the minimum point representing the equilibrium volume where the total energy is lowest, and the system is most stable. The minimum in NdCuSO is detected around a volume of 880 $(\text{a.u.})^3$ with an energy near -47030.055 R_y, indicating a relatively well-defined and symmetric energy basin, implying high structural stability with negligible anharmonic contributions. In comparison, PrCuSO displays its minimum at a slightly higher equilibrium volume, 890 $(\text{a.u.})^3$, with an energy approaching -48590.045 R_y, showing the effect of the larger ionic radius of Pr than Nd. It is a constant change to a larger optimum cell volume with the lanthanide trends of contraction, whereas the lattice is gradually distorted despite the full structural integrity being maintained by the change in the difference in the sizes of the rare-earth ionic sizes.

The difference between NdCuSO and PrCuSO is a considerably lower equilibrium volume than a longer lattice parameter, and they both exhibit smooth, symmetric curves, indicating that they are thermodynamically stable, and the structural uncertainties in the explored volume range do not influence the profiles. Even the qualitative data about the bulk modulus can be obtained with the help of the curvature of the parabola: the steeper curve of NdCuSO indicates a significantly higher rigidity and a significantly lesser compressibility, whereas the wider curve of PrCuSO demonstrates a better ability of the lattice to undergo the influence of the outside pressure. Such optimization confirms the structural parameters of the ground-state not only, but also illustrates how the replacement of Nd by Pr perturbs the equilibrium geometry and elastic response and would prove a high level of support in the future study of their electronic, optical, and thermoelectric properties. Apparently, the formation and cohesive energies calculated indicate that NdCuSO and PrCuSO are thermodynamically and structurally stable compounds. The negative formation energies of NdCuSO (-3.24 eV f.u.^{-1}) and PrCuSO (-3.46 eV f.u.^{-1}) are indications that the compounds can be prepared independently of their respective essentials in a state of equilibrium. PrCuSO is somewhat more thermodynamically stable because of the increased negative formation energy. The cohesive energies of NdCuSO (-4.21 eV f.u.^{-1}) and PrCuSO (-4.63 eV f.u.^{-1}) indicate strong interatomic bonds and stable crystal structures, with the PrCuSO exhibiting better lattice cohesion. The enormous negative energies of cohesion demonstrate that significant energy is needed to split such materials into isolated atoms, and it stresses the stability of such matter both mechanically and structurally. The contribution of the elements to the lattice stabilization and ionic bonding is mostly from the rare-earth elements (Nd/Pr), while the role of Cu is in the covalent–

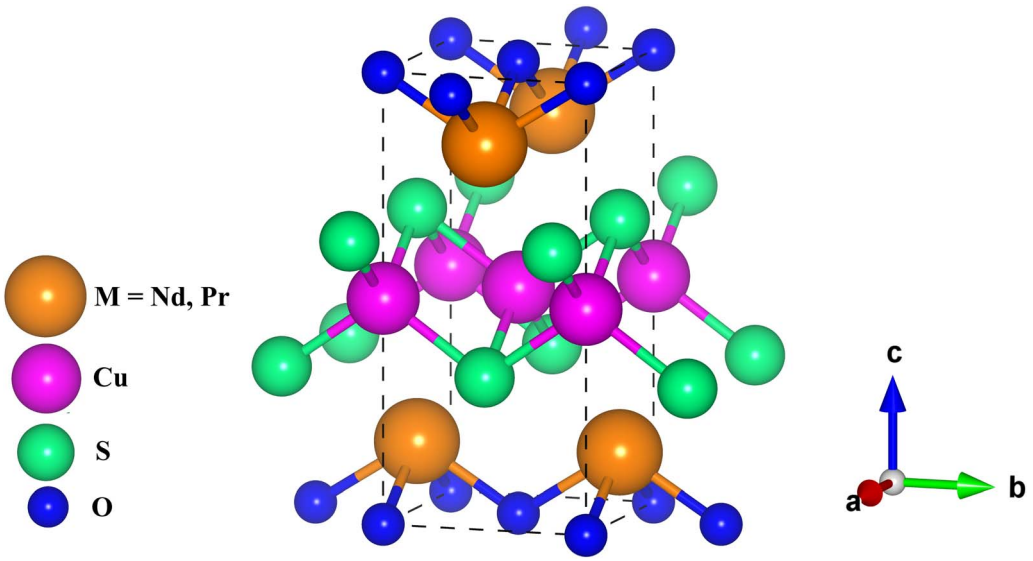

Fig. 1 The unit cell crystal structure for McuSO (M = Nd, Pr) rare earth oxychalcogenides.

metallic relations, strengthening the structure. S provides the directional covalent bonding, and O increases the overall stability with the help of strong Cu–O and rare-earth and O interactions. A combination of these properties forms NdCuSO and PrCuSO as energy-efficient and stable quaternary chalcogenide oxides.

3.2 Electronic properties

Fig. 2(a)–(d) depicts the electronic band structure of NdCuSO and PrCuSO materials in spin-up and spin-down channels, and the electronic behaviours and spin-dependent band structures of both materials can be compared. In each figure, the horizontal axis shows the high-symmetry locations in the Brillouin zone (Γ, X, M, Z, R, A) and the vertical axis denotes the electronic energy relative to the Fermi level (E_F), which is set at zero. In Fig. 2(a), illustrating NdCuSO in the spin-up case, the Fermi level overlaps with the conduction band near the X-M region, indicating metallic or degenerate semiconducting behaviour, with electrons partially occupying states immediately above E_F and the valence band maximum (VBM) below E_F. In Fig. 2(b), for NdCuSO in the spin-down channel, the conduction band is pushed higher in energy relative to E_F, resulting in an energy gap of about 1.2 eV, indicating semiconducting character; here, E_F is closer to the conduction band edge but does not overlap, indicating possible spin-polarized semiconducting behaviour. In Fig. 2(c), PrCuSO in the spin-up channel exhibits comparable features to NdCuSO, with E_F cutting through the conduction band at the X–M line, implying a metallic-like or strongly doped semiconducting nature; however, the conduction band minimum (CBM) looks slightly displaced when compared to NdCuSO. Meanwhile, in Fig. 2(d), PrCuSO in the spin-down channel mimics NdCuSO, with E_F close to but not crossing the conduction band edge, resulting in a band gap of 1.0 eV, indicating semiconductivity. The arrows in each panel indicate the spin asymmetry: spin-up channels show metallic features, while spin-down channels show semiconducting ones, resulting in half-metallic behaviour for both materials. This implies that the material acts as a conductor in one spin channel and as a semiconductor in the other, which is a valuable property in spintronics where spin-polarized currents are of great significance. Both NdCuSO and PrCuSO have the same overall half-metallic nature, though PrCuSO is found to have a narrower spin-down channel gap and flatter conduction bands, suggesting lower carrier mobility and heavier effective masses compared to NdCuSO. The presence of 4f electrons in the Nd and Pr adds to the band structure's localized states, particularly the relatively flat bands near 1 to 3 eV above E_F, which are characteristic of the rare-earth elements with localized f orbitals. These states may hybridize weakly with the O and S p-orbitals and Cu d-states, but their smoothness shows good localization with little contribution to the conduction. The small differences between NdCuSO and PrCuSO are due to the difference in the electronic configurations of Nd^{3+} ($4f^3$) and Pr^{3+} ($4f^2$) that directly depend on the f-levels and the effect of hybridization with the rest of the ligands. These small inconsistencies are manifested as small discrepancies in the conduction band positions and the effective band gaps. The fact that the band gap between the two spin channels differs is also important, as it determines the spin polarization of the two spin channels at E_F, since only one of the spin orientations can contribute to conduction, the materials can become almost 100% spin polarized, a feature of half-metals. Furthermore, the closeness of E_F to the band that holds the conduction band in the spin-down channel suggests that the external forces, including the doping, pressure, or temperature, might modify the electronic structure, which might lead to changes in the half-metallic, metallic, and semiconducting regimes.

The experimental study of spin-dependent transport application in the NdCuSO and PrCuSO has merit because they are tunable. The electronic band structure of NdCuSO and PrCuSO

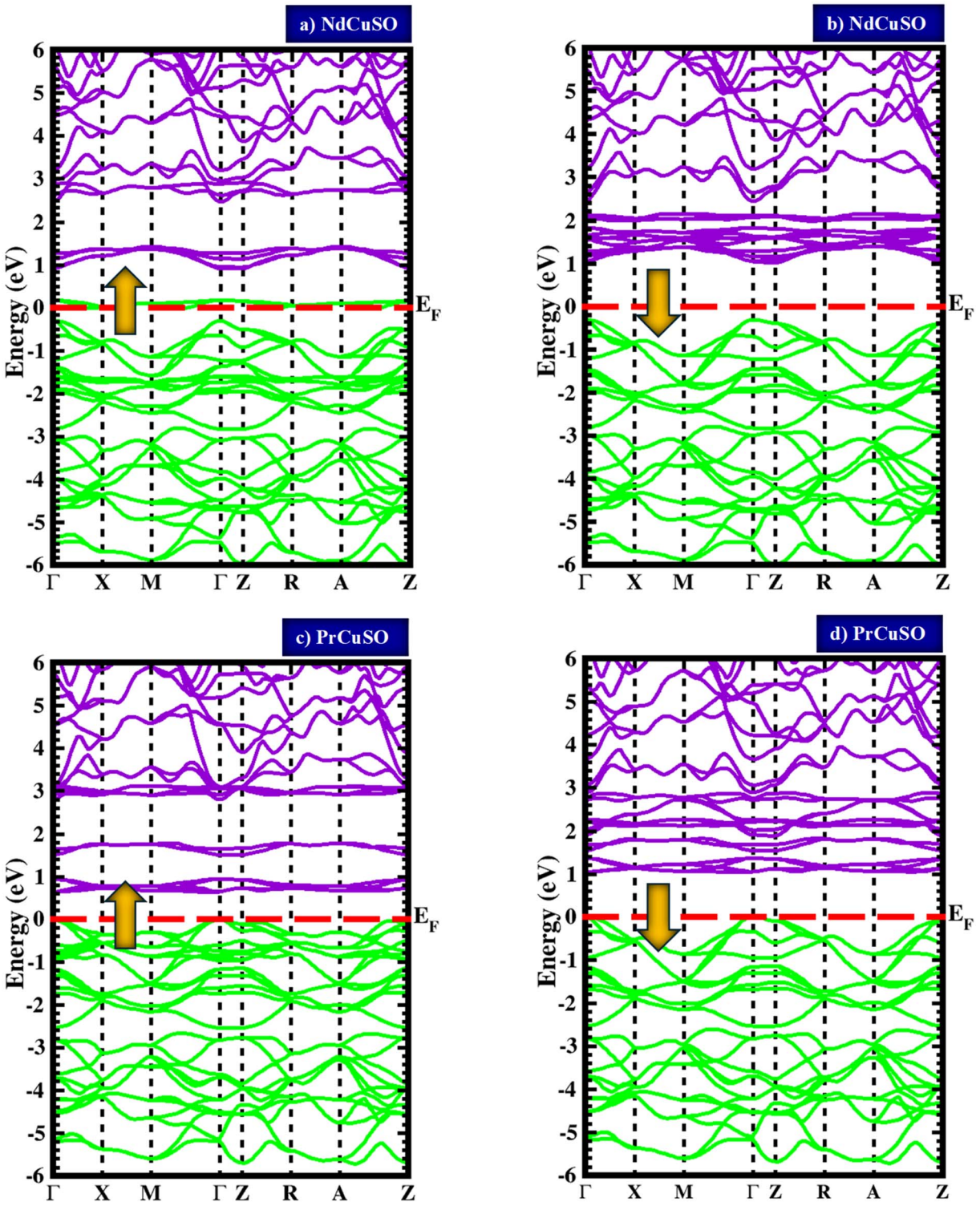

Fig. 2 The spin-polarized band profiles for (a and b) NdCuSO and (c and d) PrCuSO rare earth oxychalcogenides.

gives the prerequisite knowledge regarding the orbital contributions and spin polarization that affect their magnetic and transport properties. Nd-f states contribute the most to the conduction band of NdCuSO at 2–4 eV, which highlights the significance of the localized 4f electrons in conduction determination. Cu-d states are clumped in the −2 to 0 eV range and have a highly asymmetrical distribution overall between the spin-up and spin-down states, which is the magnetic polarization of the Fermi level. S-p orbitals are predominantly added between −4 and −2 eV, whereas O-p states predominate in the

lower part of the valence band (−5 to −2 eV), both of which are nonmagnetically active in nature. PrCuSO, conversely, shares the orbital distribution essentially uniformly with Pr-f states that bring more localization to the orbital distribution, which in both spin channels gives sharper peaks at the conduction band edge (2–4 eV). It means that 4f electrons are more localized and Pr produces a bigger effect on conduction states compared to Nd. Also, between −2.0 and 0 eV, Pr-d orbitals are more

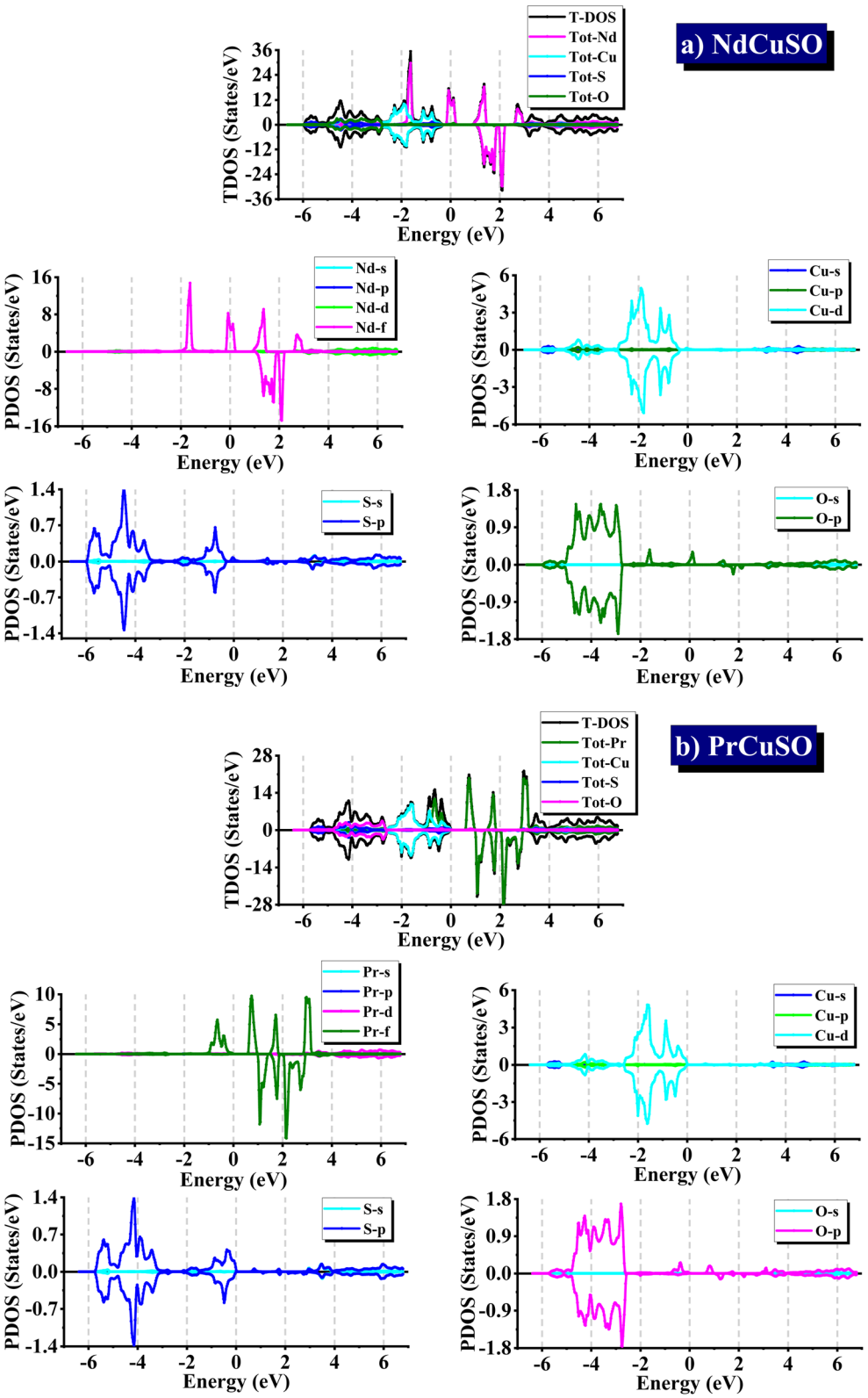

Fig. 3 The calculated density of states of (a) NdCuSO and (b) PrCuSO rare earth oxychalcogenides.

conspicuous with the Cu-d orbitals, which in turn encourages the hybrid state of Cu–Pr; however, at the Fermi level, Cu-d states are still predominant, this time, perhaps because of the spin asymmetry that triggers the magnetic ordering. Fig. 3(a) and (b) shows the total and projected TDOS and PDOS of these NdCuSO and PrCuSO that provide the detailed picture of the electronic structure, and enable an identification of orbital contributions of the electronic states of both spin-up and spin-down within them to be subsequently used to correlate their electronic, magnetic, and transport properties. In NdCuSO, TDOS displays the meaningful contribution of the Nd and Cu orbitals to the states around the Fermi level, with O and S orbitals dominating in the lower-lying valence states. The conduction band is dominated by Nd-f orbitals with the contributions lying between 1.0 eV and 3.0 eV in the two spin channels, which also fits the small nature of 4f electrons in the rare-earth ions. However, Nd-f states emerge in the valence band region between −2.0 eV and −1.5 eV and intersect the Cu-d levels, which means that hybridization is strong and that there will be the possibility of interactions between the levels and the charge transfer. The most obvious Cu-d states occur in the −2.0 eV 0 eV energy band, which is predominantly dominated by the near-Fermi valence band and shows a significant asymmetry between the spin-up and the spin-down modes.

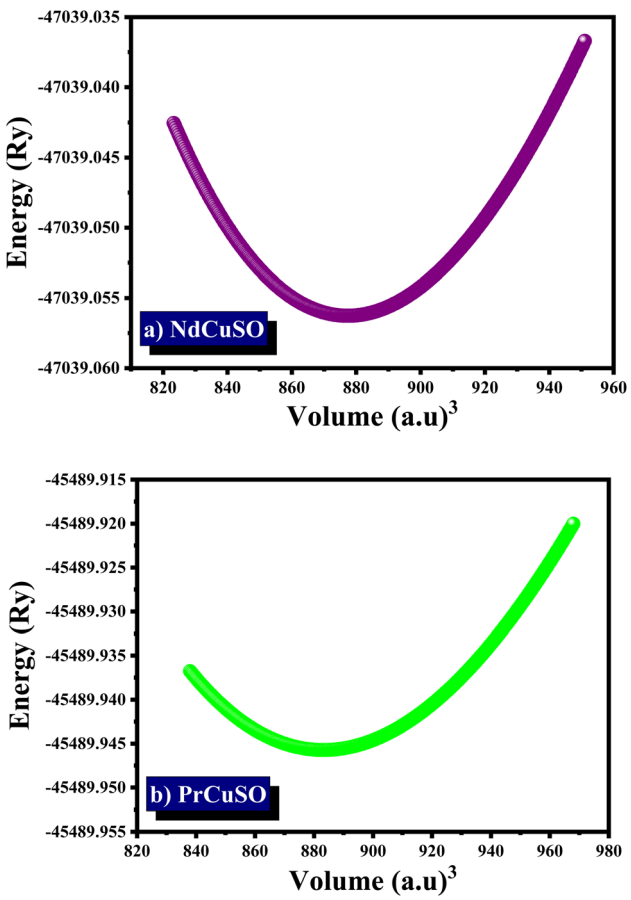

Fig. 4 The optimization plots of (a) NdCuSO and (b) PrCuSO rare earth oxychalcogenides.

Such an imbalance displays magnetic polarization, which means that the Cu is participating in spin-splitting effects.

The S-p orbitals S-p orbitals are centred between −4.0 eV and −2 eV, and though they are weaker, extend slightly lower to −6 eV. O-p states, on the contrary, have a more widespread distribution between −5 eV and −2 eV, forming the deeper valence band. O-p and S-p states appear symmetric across spin-up and spin-down channels, and this indicates that they are nonmagnetic and bonding. So, the conduction region of NdCuSO is controlled by Nd-f orbitals, but Cu-d orbitals have a significant impact on the valence states near the Fermi energy. This implies that conduction behaviour is dominated by the Nd, and the electron transport of electrons around the valence band maximum is dominated by Cu. The PrCuSO, however, has a much more widely dispersed pattern, but with the major differences being due to the replacement of Nd with Pr, which occurs with stronger and sharper peaks between 2 eV and 4 eV, which is somewhat higher than the Fermi threshold. Their further localization means that the Pr-f orbitals have a less important interaction with the rest of the states, leading to the more clearly defined electronic states and a greater impact on the conduction band. This difference demonstrates that the PrCuSO can be the most effective correlation effect compared to the NdCuSO. Pr-d orbitals are also a minor contributor between −2 eV to 0 eV overlapping with the Cu-d states and reinforcing Pr–Cu hybridization in the valence region, although smaller than in the NdCuSO. The near-Fermi region, with the particular focus on −2 eV to 0 eV, is occupied by Cu-d states, such as NdCuSO, which possesses the asymmetric structure of the spin-up and spin-down channels. This spin-spinning indicates possible magnetic ordering preference, and the Cu makes an important contribution to the magnetic ordering. S-p and O-p contributions are also similar to those observed in the NdCuSO. The S-p states are concentrated in the −4 eV to −2 eV range, but the O-p states are predominant between the −5 eV and −2 eV. The two orbitals are spin symmetric, that is, they do not contribute to the magnetism but stabilize the valence band through bonding interactions. In a comparison of the two compounds, there are some significant differences. The Nd-f states are less localized, or displaced a bit higher in energy within the conduction band in the NdCuSO, and more localized and dominate the conduction band minimum in the PrCuSO. This implies that substituting Nd by Pr enhances the f-orbital contributions, which make them more dominant in the electronic structure. Nevertheless, the Cu-d orbitals are still at the centre of both the states around the Fermi level material and hence ensure that Cu is in control of the valence band mostly. In both situations, the spin asymmetry in the states of Cu-d exists, though more in the PrCuSO, which is a higher expression of magnetic nature. The increased interaction between localized Pr-f electrons and Cu-d states is the most likely cause of this difference in spin polarization. The O-p and S-p orbitals are similar in both compounds, whose action is restricted to the deeper valence bands and does not contribute to the magnetic or transport phenomenon.

Phonon dispersion curves of NdCuSO and PrCuSO, as displayed in Fig. 5, are vital in gaining a critical insight into the

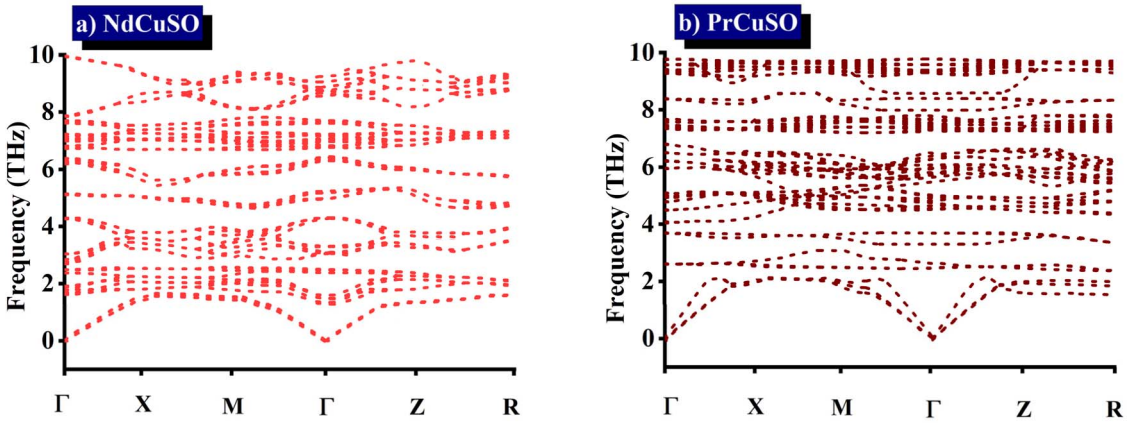

Fig. 5 The computed phonon dispersion plots of (a) NdCuSO and (b) PrCuSO rare earth oxychalcogenides.

dynamical stability of the material and the lattice vibrational behaviour. All the phonon branches of both materials are positive over the whole Brillouin zone, and no imaginary (negative) frequencies are found, indicating that they are dynamically stable and structurally robust. The acoustic branches are smoothly expanded at zero frequency at the Γ-point, with the anticipated linear dispersion, indicating good elastic behaviour and stable long-wavelength lattice vibrations. The phonon spectrum in NdCuSO is comparatively more dispersive, especially in the acoustic region, indicating higher phonon group velocities and stronger lattice interactions, which are associated with its marginally larger lattice thermal conductivity. In comparison, the phonon branches of PrCuSO are relatively flatter, particularly at low frequencies, which implies a decrease in phonon velocities and an increase in phonon scattering. Moreover, PrCuSO represents higher optical-mode clustering and a little softening around the high-symmetry points, which is stronger evidence of anharmonicity and pronounced vibrational modes because of Pr atoms presence. The frequency range of the two materials is extended to the order of 10 THz, with optical modes dominating the higher frequency range, mainly due to the lighter atoms (O and S). In comparison, NdCuSO exhibits comparatively stiffer lattice dynamics, whereas PrCuSO has better phonon scattering properties. In general, the two materials are dynamically stable, although PrCuSO is likely to have lower lattice thermal conductivity because of the weaker phonon behaviour.

3.3 Elastic properties

The elastic parameters calculated for the tetragonal NdCuSO and PrCuSO provide all the details concerning the mechanical stability, bonding properties, deformation resistance, and the structural reliability under external stress, which are fundamental to the possible applications as useful semiconducting materials. The bulk modulus B was estimated to be 87.8 GPa in the NdCuSO and 91.7 GPa in the PrCuSO (see Table 1), indicating that both materials exhibit a moderate resistance to the volume reduction under pressure applied. PrCuSO has a somewhat higher bulk modulus than NdCuSO, which is more

Table 1 The elastic coefficients, elastic moduli, bulk modulus (*B*), shear modulus, *G* (GPa), Young's modulus (Y) (GPa), Poisson's ratio (*v*), Cauchy pressure (*C*″), Pugh-ratio (*B*/*G*) and anisotropy constant (*A*) of the NdCuSO and PrCuSO quaternary oxychalcogenides

Elastic parameters	NdCuSO	PrCuSO
C_{11}	168	175
C_{12}	62	65
C_{13}	54	57
C_{33}	142	148
C_{44}	48	52
C_{66}	53	55
Bulk modulus, *B*	87.8	91.7
Shear modulus, *G*	46.2	48.7
Young's modulus, *Y*	118.2	125.6
Poisson's ratio, *ν*	0.27	0.26
Cauchy pressure, *C*″	14.0	13.0
Pugh ratio, *B*/*G*	1.90	1.88
Elastic anisotropy factor, *A*	0.91	0.95

strongly bonded with other atoms. This is due to the reduced ionic radius of Pr^{3+}, relative to that of Nd^{3+}, which results in the reduction of the bond lengths and overlapping of the orbitals of the layered oxysulfide structure. The trend is in agreement with the fact that the PrCuSO has systematically larger elastic constants, indicating a more condensed and stiffer lattice. Shear modulus *G*, which explains the resistance against the deformation at constant volume, and which can be regarded as a better measure of the mechanical strength than the bulk modulus, was measured at approximately 46.2 GPa in NdCuSO and 48.7 GPa in PrCuSO. These findings prove that the two materials are not only deformation resistant to shear, but PrCuSO is a little more rigid. The shear moduli are relatively high, suggesting a strong directional bonding, particularly in the Cu–S layers, which control the in-plane mechanical response of the tetragonal combinations, and confirm the absence of mechanical softness or instability. The modulus Y that defines the stiffness of a material under uniaxial tensile or compressive stress is predicted to be 118.2 GPa and 125.6 GPa for NdCuSO and PrCuSO, respectively, rendering both materials moderately stiff semiconductors. These are similar to the

reported results in other layered chalcogenide and oxysulfide systems, which indicate that both materials can undergo much elastic deformation before fracture. The Young modulus of PrCuSO is higher, which leads to a higher mechanical stiffness and is in good correlation with its bulk and shear moduli. The transverse strain response to the longitudinal loading, Poisson ratio, is the value of which provides an insight into the nature of interatomic bonding, and is determined to be approximately 0.27 in NdCuSO and 0.26 in PrCuSO. These are within the range of normal values of these materials, which have mixed ionic-covalent bonding, where the directional covalent bonds and the non-directional ionic interactions make equal contributions. The Poisson's ratio of PrCuSO is slightly smaller than that of the NdCuSO, indicating that the bonding is directed, with the higher stiffness and lower compressibility of PrCuSO. More importantly, the values of these ratios of Poisson in semiconducting oxysulfides are physically possible, indicating that neither is excessively brittle.

The Cauchy pressure determined as C_{12}–C_{44} is positive for both compounds, with a value of approximately 14 GPa in NdCuSO and 13 GPa in PrCuSO. The positive Cauchy pressure is typically associated with the ductile behaviour and the prevalence of non-directional bonding components, whereas negative values are characterized by large directional covalent bonding and brittleness. The observed positive Cauchy pressures indicate clearly that both NdCuSO and PrCuSO are ductile, which is applicable in real applications that require mechanical integrity at stress and defect tolerance. The presence of the stronger covalent relationships indicated by the relatively lower Cauchy pressure of PrCuSO is associated with its increased elastic stiffness. It has been calculated that the Pugh ratio B/G, which is regularly used to classify between the ductile and brittle behaviour, is 1.90 in NdCuSO and 1.88 in PrCuSO (see Table 1). As these ductile materials differ by one of the most essential values of approximately 1.75, such materials are directly defined as ductile. According to the obtained results, both materials possess an excellent ratio of fracture and plastic deformation resistance, which predetermines their mechanical strength and suitability in the building of devices, thin-film deposition, and other useful procedures. The B/G ratio of NdCuSO is slightly higher than that of PrCuSO, and the ductility of NdCuSO is marginally higher, but the difference is minute, and the two are fairly ductile. The directional dependence of the elastic behaviour and the extent of mechanical anisotropy in the crystal is indicated by the elastic anisotropy factor A. As shown in Table 1, calculated values of A of NdCuSO and PrCuSO are approximately 0.91 and 0.95, respectively, and a significant anisotropy of elasticity is evident in both materials. The elastic isotropy is associated with a value of unity, whereas an anisotropic mechanical response is indicated by a non-unity value. This is not surprising as the tetragonal structure, and there is a strong in-plane bonding, which is accompanied by weak interlayered bonding along the c-axis. Having an anisotropy factor closer to unity, PrCuSO exhibits rather homogeneous elastic behaviour in various crystallographic directions, with increased mechanical homogeneity. The shear constant C', defined as $(C_{11} - C_{12})/2$, determines resistance to tetragonal shear deformation and helps as an extra criterion for mechanical stability. C' values were determined to be about 53.0 GPa for NdCuSO and 55.0 GPa for PrCuSO (see Table 1), which are both large and positive, showing considerable resistance to shear distortion within the basal plane and further approving the mechanical stability of these materials. PrCuSO has the principal C, so its rigidity and bond strength are illustrated. On the whole, when all elastic parameters are compared, it is possible to note that both NdCuSO and PrCuSO are mechanically stable, ductile, and rather stiff tetragonal semiconductors. Still, PrCuSO always exhibits a little better mechanical characteristic, such as the higher bulk modulus, Young's modulus, shear modulus, and anisotropy factor, which is often near unity, and shear constant. These are potentially because of minor changes in ionic size, strength of bonding and lattice compactness as a result of Nd replacement with Pr. However, both materials possess excellent mechanical consistency, strong ductility and average anisotropy in elasticity of material, which makes them good future candidates in the realm of optoelectronic, thermoelectric, and other operational applications that require both semiconducting properties and mechanical stability of the material that need a combination of semiconducting characteristics and mechanical durability.

3.4 Optical properties

Fig. 6(a) shows the real dielectric function, $\varepsilon_1(\omega)$, for NdCuSO and PrCuSO. Both materials have high static dielectric values at zero photon energy, indicating strong polarization and efficient dielectric screening in the low-energy domain. This large response is due to interband transitions at and around the fundamental absorption edge, where the electrons are excited out of O-2p and S-3p valence states into the conduction states, which are mainly occupied by Cu-3d and rare-earth orbitals (Nd-4f/5d, Pr-4f/5d). The maximum value of $\varepsilon_1(\omega)$ for NdCuSO is a little larger than that of PrCuSO. The polarizability is better, the dielectric screening is better, and the value of the static dielectric constant is a little larger. Beyond 3 eV photon energy, $\varepsilon_1(\omega)$ becomes smaller. The major oscillations are located in the 4–9 eV range, which exhibit resonant interband transitions with the locations that are important in the electronic band structure. At energies above 10 eV, the curves of the two materials level off and tend to zero, indicating that the electronic polarization of atoms plays a small role in the interaction of photons and matter at high energies, where the lower core states dominate. The NdCuSO and PrCuSO $\varepsilon_1(\omega)$ spectra resemble each other, indicating that the Pr replacement of Nd does not have a significant impact on the optical response. Nevertheless, the slight variation in the scale indicates the influence of the size of rare-earth cations and the local character of 4f electrons on the dielectric screening. This comparison may indicate that, although the two oxysulfides exhibit virtually the same dielectric properties, NdCuSO could be a little better dielectrically, so that it can be used in such applications that demand a higher polarization response and higher screening in optoelectronic and photonic devices. Fig. 6(b) displays the imaginary dielectric function, $\varepsilon_2(\omega)$, that reveals the behaviour of photon absorption

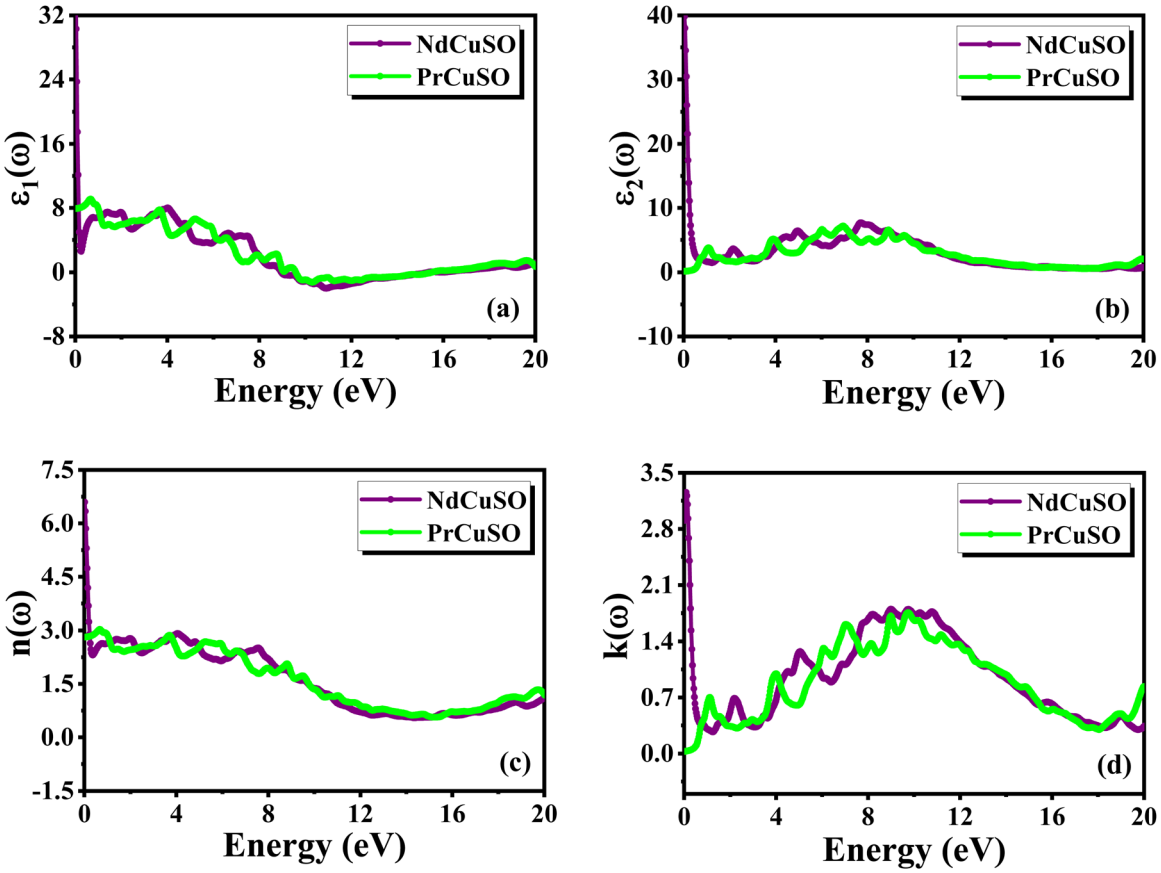

Fig. 6 The calculated (a) real component, (b) imaginary component, (c) refractive index, (d) extinction coefficient, McuSO (M = Nd, Pr) rare earth oxychalcogenides.

and the onset of interband transitions of NdCuSO and PrCuSO that provide a direct connection to their optical behaviour. The two materials show a sharp peak at low energies (less than 2 eV), which is related to the basic absorption edge, which reflects their direct band gap semiconducting character. The $\varepsilon_2(\omega)$ grows rapidly as a result of electronic excitations between conduction and valence bands, and the intensity of the peak depends on the density of states and the interband transition probability. The NdCuSO has moderately higher peaks in the low-energy region than PrCuSO, indicating that it has more observable optical transitions near the band edge, which could enhance absorption in the visible and near-UV spectral regions. With increasing photon energy, both materials indicate the multiple secondary peaks reaching up to approximately 10 eV, indicative of the transitions of deeper valence states, mainly O-2p and S-3p orbitals, which are hybridized with the occupied Cu-3d, to the higher occupied conduction states, including Cu-3d and rare-earth d/f states. Such peaks testify to the complicated electronic structure and the significance of localized orbital in optical excitations. Above 12 eV, the $\varepsilon_2(\omega)$ becomes sub-exponential in nature, and it serves as the value of zero, indicating that the contribution of higher-energy photons to additional interband transitions is minimal because few electronic states are available. The $\varepsilon_2(\omega)$ values of NdCuSO are slightly greater in the low-intermediate energy region, which means that they have better absorption efficiency and optical responsiveness than PrCuSO.

Fig. 6(c) displays the spectrum of $n(\omega)$, which provides a complete picture of the light–matter interaction in these NdCuSO and PrCuSO, not only by directly being a result of the real and imaginary components of the dielectric function but also directly affecting the speed of light propagation and the degree to which light is bent within the material. These two materials have high values of static refractive index at zero photon energy, with NdCuSO a bit higher than PrCuSO, as the latter has a higher value of the static dielectric constant, $\varepsilon_1(0)$. This implies that the electromagnetic waves travel at a slower pace in the NdCuSO, and this proves that NdCuSO has a better dielectric response compared to PrCuSO. With increasing photon energy, a gradual fall of $n(\omega)$ indicates that there is much normal dispersion in the low-energy region (6 eV), principally due to resonant interband transitions. The refractive index decreases further past this range, approaching unity in photon energies exceeding 15 eV. That demonstrates that the two materials become almost transparent to high-energy photons, as the possibility of the optical transitions reduces. These materials exhibit rhythmic variability of $n(\omega)$ between 4 and 10 eV that are very similar to the absorption-related peaks in the dielectric function. It confirms the interplay between the refractive behaviour and resonant optical transitions between

O-2p, S-3p and Cu-3d orbitals. Notably, NdCuSO has a slightly higher refractive index through the spectral range, suggesting a better optical confinement, higher phase retardation, and high-index-contrast photonic applications, including waveguides, dielectric coating, and high-index-contrast photonic devices. PrCuSO, however, has a little lower refractive index and weaker dispersion, which means that it has lower optical delay and birefringence and thus is more easily applied in samples that demand low optical distortion. Therefore, this comparison shows that NdCuSO is superior in high confinement optical applications, even though PrCuSO is superior in the reduction of light distortion. Fig. 6(d) presents the spectrum of the extinction coefficient $k(\omega)$ that will provide immediate evidence related to the reduction of electromagnetic waves within NdCuSO and PrCuSO. It quantifies photon absorption and highly overlaps with the $\varepsilon_2(\omega)$. Both materials exhibit a rapid onset in the $k(\omega)$ around the band edge, then a distinct peak below 2.0 eV, demonstrating the fundamental absorption edge and confirming their direct band gap semiconductivity. This low-energy range absorption is due to the electronic excitations across the band gap, and the larger extinction peak at NdCuSO than at PrCuSO demonstrates its improved absorption capacity at visible-light-driven optoelectronic applications. At increased energy (high photon energy), both materials demonstrate increased extinction behaviour between 6 and 12 eV, which represents more energetic interband transitions involving deeper valence orbitals (O-2p and S-3p hybridized states) to the empty Cu-3d and rare-earth d/f conduction states. PrCuSO exhibits slightly higher extinction values in this intermediate energy band when compared with NdCuSO, which means that Pr substitution is more effective in absorbing optical energy that is associated with higher electron states. On the part of these two materials, $k(\omega)$ is smaller than at lower eV because higher photon energies suppress the optical transitions and increase transparency. This relative discussion shows that both NdCuSO and PrCuSO are effective absorbers in the visible and ultraviolet spectral ranges, but with complementary strengths: NdCuSO has a weak edge at the 1. Basically, the absorption edge, so it is likely to be used in band-edge optical applications, and PrCuSO has a strong edge at higher photon energies, so it is likely to be used in processes that require the more intense UV absorption. These findings justify the adjustable optical properties of these oxychalcogenides for some optoelectronic device applications.

Fig. 7(a) illustrates the optical conductivity for NdCuSO and PrCuSO, which can be used to interpret their photoconductive behaviour and the dynamics of charge carriers in photon excitation. The spectra indicate that both materials have negligible conductivity in low photon energy (<1 eV), which indicates infrared-visible transparency and makes them semiconducting materials with a finite band gap. A steep onset of the

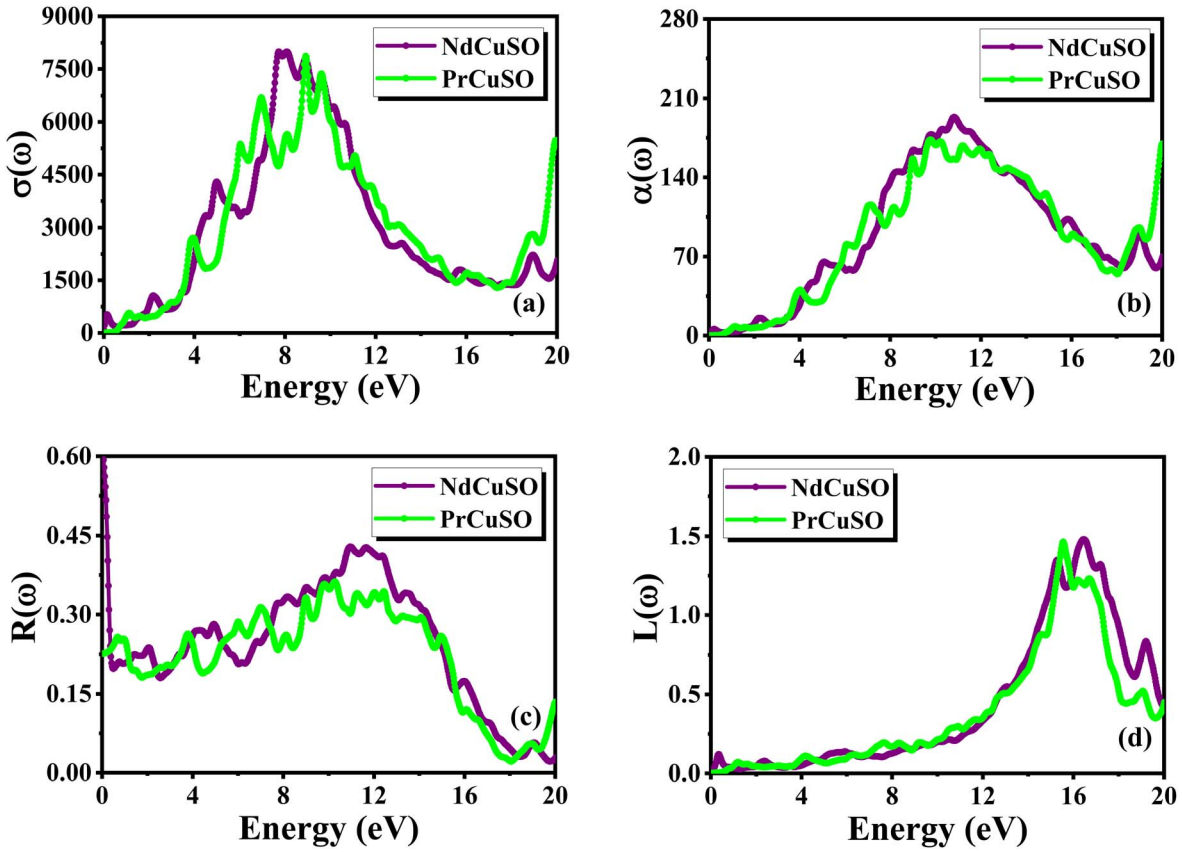

Fig. 7 The calculated (a) real optical conductivity, (b) absorption coefficient, (c) reflectivity, and (d) energy loss function for McuSO (M = Nd, Pr) rare earth oxychalcogenides.

conductivity can be observed at the absorption edge as photon energy increases, indicating the threshold at which interband transitions can occur, whereby electrons are excited out of the occupied states in the valence band to empty states in the conduction band. This is succeeded by the steep peaks in the 7 to 10 eV range, which are due to the strongest interband transitions and are probably caused by the hybrid O-2p/S-3p to Cu-3d and the infrequent rare-earth 4f/5d states. It is important to emphasise that PrCuSO is a little more conductive at room temperature than NdCuSO, indicating that Pr substitution is beneficial to photoconductive response when it is necessary to convert the charge carriers into the sample and move them more efficiently, which is explained by the minor differences in orbital overlap and electronic band structure. Above 10 eV, the conductivity decreases continuously but is not zero until 20 eV, suggesting more transitions of higher intensity but with a lower intensity. The total behaviour demonstrates that these materials are very absorbing and reactive to the UV light, and the fact that it is highly conductive in this fraternity makes them good materials in the optoelectronic uses of UV photodetectors, transparent conducting layers, and solar energy conversion systems. As Fig. 7(b) demonstrates, the absorption coefficient of NdCuSO and PrCuSO indicates that the photon absorption and interband electronic transitions were active. The two materials also have a minor absorption answer at low photon strength (<1 eV) and thus they are transparent on the infrared scale, also revealing that they are semiconductors with discrete band gaps. Its maximum absorption coefficient is at 7–12 eV, corresponding to the sharpest interband transitions and the previously determined peaks in the 2nd derivative of the $\varepsilon_2(\omega)$, *versus* frequency and optical conductivity. This association suggests that the optical absorption results from transitions from the O-2p and S-3p states into empty Cu-3d and rare-earth f/d orbitals. When comparing the two materials, NdCuSO has somewhat higher peak absorption values than PrCuSO, suggesting that Nd substitution improves photon–electron coupling and leads to higher optical absorption efficiency, which is useful for optoelectronic applications requiring high light-harvesting capability. Beyond 12 eV, $\alpha(\omega)$ steadily drops, showing a lower probability of interband transitions at higher photon energy. Fig. 7(c) displays the reflectivity spectrum $R(\omega)$ for NdCuSO and PrCuSO, which offers useful information on the interaction of incident light with the material surfaces and supports the absorption and these conductivity investigations.

The two materials are not highly reflective (value less than 0.3) at low photon energies and in the visible range. This implies that most incident photons would pass through the materials instead of bouncing back, and so, their optical transparency in this spectrum is accepted. This behaviour is highly desirable in the optoelectronic and solar energy applications since low surface reflection guarantees effective absorption of photons within the bulk. With the growing photon energy, the value of $R(\omega)$ grows steadily and oscillates until the height of 12 eV, displaying significant interband transitions which change the optical response. Further outside this region, the reflectivity goes down again, implying that there is less photon–electron interaction when the excitation energy is higher. One subtle yet notable distinction between the two materials is that NdCuSO has a very slightly higher reflectivity in the 8 to 12 eV region than PrCuSO, which suggests that Nd substitution promotes surface photon backscattering in the high-energy ultraviolet. This disparity implies that NdCuSO may not be adapted to be applied in other applications where low UV reflectance is required; however, it could be employed in the fabrication of reflective finishes or optical reflective mirrors for select high-energy optical equipment. PrCuSO, on the other hand, is less reflective, enabling the greater penetration of photons and is slightly more desirable in applications such as solar absorbers and photodetectors, which require unattenuated absorption to work. Importantly, these two properties (low reflectivity at visible frequencies and large absorption at those frequencies) indicate that these two materials can be used as solar absorber layers and optoelectronic devices, as well as in energy conversion technologies where lower reflection losses would be directly proportional to higher efficiency. Fig. 7(d) represents the energy loss function $L(\omega)$ of NdCuSO and PrCuSO. It measures the energy dissipated by high velocity electrons passing through the material and directly measures plasma oscillations and collective electronic excitations. In both materials, the 15 to 18 eV range exhibits clearly defined peaks, which are related to the fact that the 15 to 18 eV are the plasma resonance frequency due to the collective oscillation of the valence electron density. The sharp plasmon peaks suggest the occurrence of metallic-like excitation behaviour at increased photon energy. This conforms to argument 1 that the real function of the dielectric $\varepsilon_1(\omega)$ decreases towards zero and the imaginary function $\varepsilon_2(\omega)$ peaks simultaneously to fulfil the plasma resonance condition. A major distinction between the two materials is that NdCuSO has a slightly higher energy than PrCuSO, which implies that NdCuSO has a slightly higher plasmonic response and a higher effective plasma frequency. The difference in electronic structure and electron density can be small (due to the substitution of the rare-earth), and this can result in the Nd making large collective oscillations of the valence electron gas compared to Pr. The strength of the peaks also suggests that both materials lose significant energy in this regime, which is important in establishing their eligibility for plasmonic and high-energy photonic applications. The strong plasmon resonances demonstrate that, whereas NdCuSO and PrCuSO behave as semiconductors at low energies, their high-energy optical response has metallic-like properties due to collective excitations.

3.5 Thermoelectric properties

Fig. 8(a) shows the Seebeck coefficient S of NdCuSO and PrCuSO, with the S values being negative in the anisotropic range studied, which is a characteristic that makes those two materials n-type materials with the electrons being the majority carriers. Seebeck coefficient is a reflection of the amount of entropy transferred by a charge carrier, and it is directly proportional to the concentration of the carrier. NdCuSO is approximately -6.5 μV K^{-1} at 300 K, whereas PrCuSO is slightly lower at -7.2 μV K^{-1}. It implies that the electron density or the more intense scattering effects of PrCuSO can be much higher, which leads to a larger

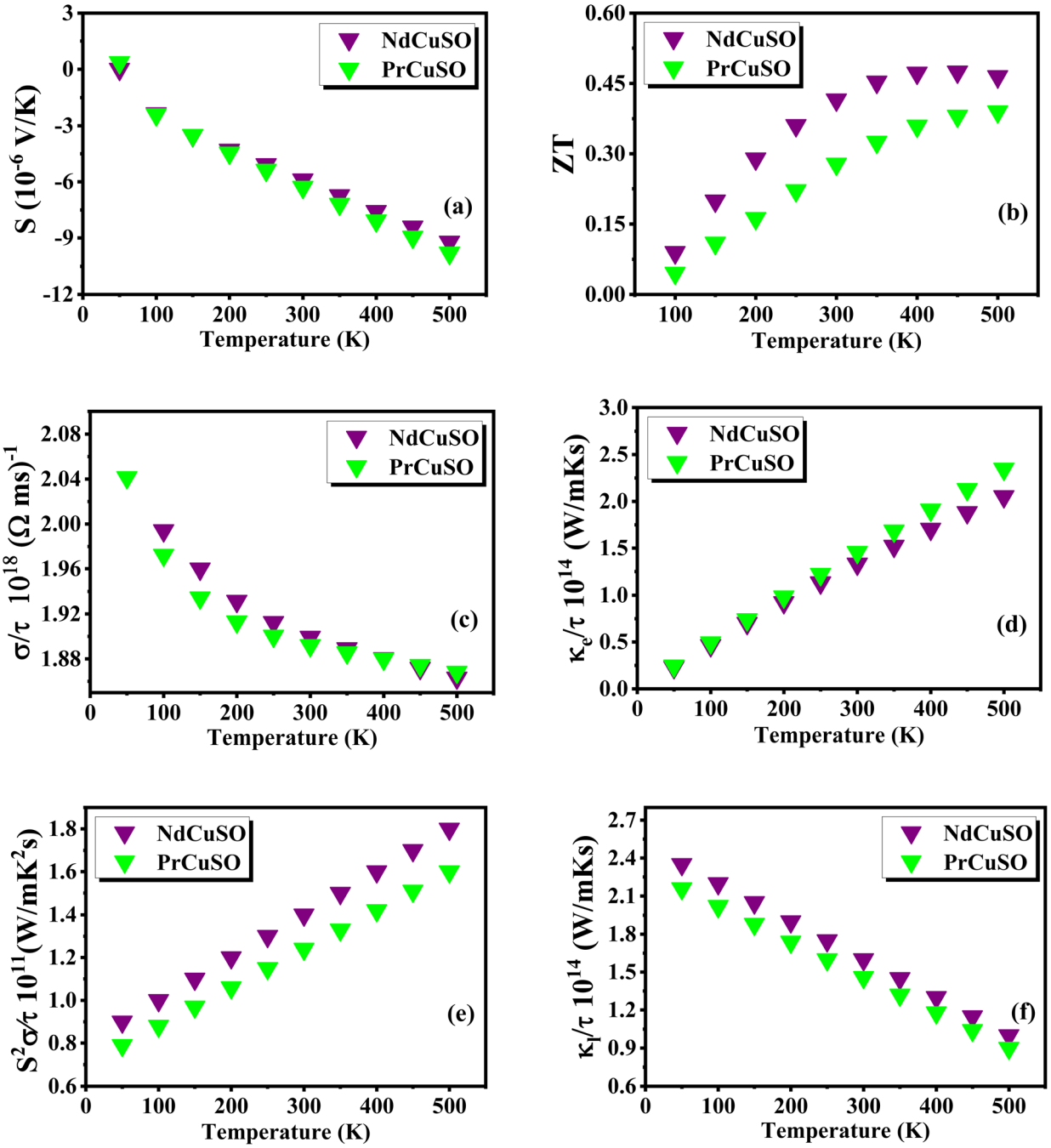

Fig. 8 The calculated (a) Seebeck coefficient, (b) figure of merit, (c) electrical conductivity, (d) electronic thermal conductivity, (e) power factor, and (f) lattice thermal conductivity, MCuSO (M = Nd, Pr) rare earth oxychalcogenides.

thermopower. S drops monotonically with increasing temperature for both compounds, reaching -9.2 μV K^{-1} for NdCuSO and -10.3 μV K^{-1} for PrCuSO at 500 K. This declining tendency is well known. As the temperature rises, intrinsic excitations generate more carriers, reducing the energy difference between the Fermi level and the conduction band edge, and therefore lowering the Seebeck coefficient. Furthermore, in degenerate semiconductors, S frequently falls with T due to increasing carrier degeneracy and phonon scattering effects. The fact that PrCuSO has a continuously larger negative S than NdCuSO suggests that Pr-based compounds either have a higher density of states effective masses or stronger electron localization, both of which increase thermopower in the negative direction. The relatively low values (-7 to -10 μV K^{-1}) of Seebeck coefficients reported in this present study are rather low in comparison with the values of conventional thermoelectric materials. The low Seebeck coefficient occurs due to high carrier concentration and Fermi level closeness to the conduction band, which naturally limits thermopower despite adequate electrical conductivity. This is, however, in line with the degenerate or highly doped

semiconducting/half-metallic character of NdCuSO and PrCuSO in the electronic structure analysis. In these systems, the Fermi level is either very near or within the conduction band (in one spin direction), resulting in large carrier concentrations, which in turn causes a negative Seebeck coefficient according to transport theory. In this way, the values obtained are physically reasonable and typical for the materials that have metallic or half-metallic transport behaviour, as opposed to the intrinsic semiconductors. In Fig. 8(b), the thermoelectric figure of merit (ZT) for NdCuSO and PrCuSO varies with temperature. This provides an integrated measure of efficiency by combining the effects of the Seebeck coefficient (S), electrical conductivity (σ), and thermal conductivity (κ) through the relation $ZT = S^2\sigma T/\kappa$. Both materials show a steady increase in ZT with increasing temperature, as is usual for semiconducting thermoelectrics working in the intrinsic domain. NdCuSO has a higher ZT of approximately 0.32 at 300 K compared to PrCuSO, which has approximately 0.25, meaning that NdCuSO has a better balance of transport properties at normal temperature. The increased trend with temperature is due to the linear dependency on T in the numerator and the squared contribution of the Seebeck coefficient, which surpasses the reductions in S and σ with greater phonon scattering. However, κ does not climb steeply enough to counteract this gain. At 500 K, the ZT values had increased substantially with NdCuSO and PrCuSO now at approximately 0.48 and 0.41, respectively, meaning that the greater the thermal excitation, the better its overall thermoelectric proficiency. The NdCuSO has a higher effective power factor and a higher level of electrical conductivity with a lower electronic thermal conductivity in comparison to the PrCuSO, giving it a better ZT. This advantageous mix allows NdCuSO to have a moderate thermoelectric response with an increase in temperature, giving it a great edge over PrCuSO.

Fig. 8(c) shows how electrical conductivity σ/τ depends on temperature in NdCuSO and PrCuSO. The trend illustrates the suitable phonon-constrained transport of semiconducting thermoelectric materials. At 300 K, both compounds have excellent electrical conductivity, although NdCuSO has a slightly higher value of 2.0×10^{18} $(\Omega\ \mathrm{ms})^{-1}$ compared to 1.95×10^{18} $(\Omega\ \mathrm{ms})^{-1}$ for PrCuSO, indicating somewhat greater carrier transport in NdCuSO. At 500 K, σ/τ reduces monotonically to 1.89×10^{18} $(\Omega\ \mathrm{ms})^{-1}$ for NdCuSO and 1.86×10^{18} $(\Omega\ \mathrm{ms})^{-1}$ for PrCuSO. This adverse effect is consistent with higher electron–phonon interactions at high temperatures: lattice vibration increases worsen phonon scattering, affect carrier mobility, and therefore conductivity, although slightly faster carrier excitation could be possible. Whereas σ/τ of NdCuSO remains significantly greater over the entire temperature range, meaning the electrons are less scattered, this could be due to a reduced effective mass of to, as well as a smaller degree of localization effects, which makes NdCuSO more mobile than PrCuSO. Such a small and yet important difference in electrical conductivity of the two substances is directly related to the superior ability of NdCuSO to act as a thermoelectric device. Fig. 8(d) also shows the dependence of electronic thermal conductivity (κ_e/τ) and temperature in NdCuSO and PrCuSO, indicating the presence of electron-mediated heat conduction. At 300 K, κ_e/τ of NdCuSO is approximately 1.2×10^{14} W K^{-1} m^{-1} s^{-1}, and PrCuSO has a slightly lower value of approximately 1.1×10^{14} W K^{-1} m^{-1} s^{-1}, indicating that both of them have slightly comparable but low amounts of electronic heat conductivity at ambient temperature. At 500 K, κ_e/τ continuously increases for both materials, reaching about 2.0×10^{14} W K^{-1} m^{-1} s^{-1} for NdCuSO and 2.2×10^{14} W K^{-1} m^{-1} s^{-1} for PrCuSO. Although σ drops with temperature due to increased phonon scattering and less carrier mobility, temperature has a multiplicative effect, resulting in a net rise of κ_e. At higher temperatures, PrCuSO has a slightly higher κ_e, indicating a stronger carrier contribution to heat transport. However, this is detrimental to thermoelectric performance as higher electronic thermal conductivity leads to increased heat leakage and reduces the temperature gradient needed for effective power generation. NdCuSO has somewhat lower κ_e values than PrCuSO at high temperatures, which improves its thermoelectric figure of merit ZT by retaining thermal gradients better.

The NdCuSO and PrCuSO power factor rise slowly with temperature (see Fig. 8(e)), meaning that the thermoelectric nature is optimized at high temperatures. The cause of this trend has been the combined effect of the increased degree of carrier excitation and the relatively constant electrical conductivity despite the increased phonon scattering. This has a higher power factor of NdCuSO than PrCuSO within the whole range of temperature, *i.e.*, a more favourable tradeoff of electrical conductivity and Seebeck coefficient. This can be attributed to the carrier movement increased and the conductivity of NdCuSO increased in a relative mode, as was presented in transport analysis. PrCuSO also acts the same way, but having a lower power factor means that the charge transport efficiency is also less, possibly due to stronger localization of the Pr-4f electrons. Their semiconducting nature and their usability in moderate-temperature thermoelectric usage are reflected in the trend of the rising trend in their two materials. Overall, NdCuSO has an improved performance of electronic transport, and PrCuSO has a moderate thermoelectric response in the temperature range of operation. Lattice thermal conductivity (κ_l) for NdCuSO and PrCuSO (see Fig. 8(f)) shows a distinct decreasing pattern with the rise of temperature between 0 K and 500 K, which is typical of phonon-dominated heat transport in crystalline solids. At lower temperatures, NdCuSO exhibits a marginally larger κ_l than PrCuSO, implying comparatively greater stiffness of the lattice as well as more efficient propagation of phonons. At higher temperatures, κ_l reduces markedly with temperature because of increased phonon–phonon Umklapp scattering, which inhibits heat conduction. The decrease is more significant at elevated temperatures, which validates significant anharmonic lattice interactions. Compared to PrCuSO, PrCuSO exhibits lower values of κ_l throughout the temperature profile, indicating a higher phonon scattering, probably due to more lattice distortion and mass variation caused by Pr atoms. It has a low thermal conductivity, which is beneficial in thermoelectric use, due to its ability to retain a temperature gradient. Generally, both of the materials display a similar thermal transport characteristic, but PrCuSO would be more effective in reducing lattice heat conduction; thus, it is more desirable in terms of thermal insulation.

4. Conclusions

In the present investigation, the multifunctional properties of NdCuSO and PrCuSO oxychalcogenides were thoroughly investigated through GGA+U-based first-principles calculations. Both materials have been demonstrated to be structurally stable in the tetragonal phase, producing alternating CuS and rare-earth-oxygen layers with consistent Cu–S bond lengths of 2.42 Å and Nd–O/Pr–O bonds of 2.32/2.35 Å. There are clear minima in the energy–volume curves with NdCuSO stabilizing at a somewhat lower equilibrium volume than PrCuSO, and negative formation and cohesive energies demonstrate that they are thermodynamically stable. Electronic investigation indicates that these two systems have a half-metallic behaviour: the spin-up case is metallic with crossings of the Fermi level, whereas the spin-down case is semiconducting with band gaps of 1.2 eV (NdCuSO) and 1.0 eV (PrCuSO). The Cu-3d states control the valence band, the 4f states of the rare-earth element occupy the conduction bands region, and the O-2p/S-3p orbitals stabilize the lower valence bands, resulting in a high level of spin polarization. Results indicate that the two compounds are mechanically stable, moderately stiff (Y = 118–126 GPa) and ductile (B/G of 1.9, positive Cauchy pressure), as well as elastic anisotropic. PrCuSO is a little less malleable. They have large values of the low-origin dielectric constants, strong low-energy interband transitions, low values of the visible reflectivity, strong absorption of the ultimate Violet-frequency 7 eV and 12 eV transitions, and the plasmon resonances at 15 eV and 18 eV, which are the basis of their optoelectronic capability. These two materials are both thermoelectrically n-type semiconductors, and their Seebeck coefficients are negative and tend to increase with temperature, but ZT rises gradually up to 500 K, making NdCuSO the material required in spin-dependent thermoelectric and optoelectronic devices.

Conflicts of interest

The authors have no conflicts of interest.

Data availability

Data are available upon request from the corresponding author.

Acknowledgements

This work was supported and funded by the Deanship of Scientific Research at Imam Mohammad Ibn Saud Islamic University (IMSIU) (grant number IMSIU-DDRSP2603).

References

1 X. Zhang, J. Chen, F. Wang, X. Chen, H. Ma, D. Li, C. Liu and H. Guo, *Ceram. Int.*, 2019, **45**, 11136–11140.
2 J. Chen, X. Zhang, S. Zhu, H. Ma, X. Li, H. Yu and F. Wang, *Ceram. Int.*, 2020, **46**, 8575–8581.
3 V. Johnson and W. Jeitschko, *J. Solid State Chem.*, 1974, **11**, 161–166.
4 L.-D. Zhao, J. He, D. Berardan, Y. Lin, J.-F. Li, C.-W. Nan and N. Dragoe, *Energy Environ. Sci.*, 2014, **7**, 2900–2924.
5 M. Palazzi, C. Carcaly and J. Flahaut, *J. Solid State Chem.*, 1980, **35**, 150–155.
6 J. Li, J. Sui, Y. Pei, C. Barreteau, D. Berardan, N. Dragoe, W. Cai, J. He and L.-D. Zhao, *Energy Environ. Sci.*, 2012, **5**, 8543.
7 Y.-L. Pei, J. He, J.-F. Li, F. Li, Q. Liu, W. Pan, C. Barreteau, D. Berardan, N. Dragoe and L.-D. Zhao, *NPG Asia Mater.*, 2013, **5**, 47.
8 P. Shukla, S. Nath, G. Wang, X. Shen and J. Lawrence, *J. Eur. Ceram. Soc.*, 2017, **37**, 5135.
9 D. Zou, S. Xie, Y. Liu, J. Lin and J. Li, *J. Mater. Chem. A*, 2013, **1**, 8888.
10 J. Yang, G. Yang, G. Zhang and Y. X. Wang, *J. Mater. Chem. A*, 2014, **2**, 13923.
11 D. D. Fan, H. J. Liu, L. Cheng, J. Zhang, P. H. Jiang, J. Wei, J. H. Liang and J. Shi, *Phys. Chem. Chem. Phys.*, 2017, **19**, 12913–12920.
12 R. Viennois, P. Hermet, M. Beaudhuin, J.-L. Bantignies, D. Maurin, S. Pailhès, M. T. Fernandez-Diaz, M. M. Koza, C. Barreteau, N. Dragoe and D. Bérardan, *J. Phys. Chem. C*, 2019, **123**, 16046–16057.
13 H. Mebarki, O. Arbouche, A. Zenati, S. Chibani, M. Belabbas, Y. Azzaz and B. Belgoumene, *Comput. Condens. Matter*, 2021, **27**, 00529.
14 Y. Liu, L.-D. Zhao, Y. Liu, J. Lan, W. Xu, F. Li, B.-P. Zhang, D. Berardan, N. Dragoe, Y.-H. Lin, C.-W. Nan, J.-F. Li and H. Zhu, *J. Am. Chem. Soc.*, 2011, **133**, 20112–20115.
15 Z. Wang, K. Chen, Y. Xu, Z. Wang, L. Kong, S. Wang and W.-S. Su, *Phys. Chem. Chem. Phys.*, 2025, **27**, 4766–4774.
16 A. P. Novitskii, V. V. Khovaylo and T. Mori, *Nanobiotechnol. Rep.*, 2021, **16**, 294–307.
17 H. Kang, J. Li, Y. Liu, E. Guo, Z. Chen, D. Liu, G. Fan, Y. Zhang, X. Jiang and T. Wang, *J. Mater. Chem. C*, 2018, **6**, 8479–8487.
18 F. Li, J.-F. Li, L.-D. Zhao, K. Xiang, Y. Liu, B.-P. Zhang, Y.-H. Lin, C.-W. Nan and H.-M. Zhu, *Energy Environ. Sci.*, 2012, **5**, 7188.
19 J. Sui, J. Li, J. He, Y.-L. Pei, D. Berardan, H. Wu, N. Dragoe, W. Cai and L.-D. Zhao, *Energy Environ. Sci.*, 2013, **6**, 2916.
20 N. Zhang, J. Sun and H. Gong, *Coatings*, 2019, **9**, 137.
21 S. Tippireddy, P. K. D S, S. Das and R. C. Mallik, *ACS Appl. Energy Mater.*, 2021, **4**, 2022–2040.
22 J. He, Z. Yao, V. I. Hegde, S. S. Naghavi, J. Shen, K. M. Bushick and C. Wolverton, *Chem. Mater.*, 2020, **32**, 8229–8242.
23 J. K. Harada, N. Charles, K. R. Poeppelmeier and J. M. Rondinelli, *Adv. Mater.*, 2019, **31**, 1805295.
24 A. M. Kusainova, P. S. Berdonosov, L. G. Akselrud, L. N. Kholodkovskaya, V. A. Dolgikh and B. A. Popovkin, *J. Solid State Chem.*, 1994, **112**, 189–191.
25 D. Liu, K. Cao, H. Zeng, H. Peng, F. Liu and R. Sa, *Mater. Today Chem.*, 2026, **52**, 103419.
26 D. Berardan, J. Li, E. Amzallag, S. Mitra, J. Sui, W. Cai and N. Dragoe, *Mater*, 2015, **8**, 1043–1058.

27 A. P. Richard, J. A. Russell, A. Zakutayev, L. N. Zakharov, D. A. Keszler and J. Tate, *J. Solid State Chem.*, 2012, **187**, 15–19.
28 H. Hiramatsu, T. Kamiya, T. Tohei, E. Ikenaga, T. Mizoguchi, Y. Ikuhara, K. Kobayashi and H. Hosono, *J. Am. Chem. Soc.*, 2010, **132**, 15060–15067.
29 S. K. Karna, C.-W. Wang, C.-M. Wu, C.-K. Hsu, D. Hsu, C.-J. Wang, W.-H. Li, R. Sankar and F.-C. Chou, *J. Phys.: Condens. Matter*, 2012, **24**, 266004.
30 T. Le Bahers, S. Haller, T. Le Mercier and P. Barboux, *J. Phys. Chem. C*, 2015, **119**, 17585–17595.
31 T. Le Bahers, M. Rérat and P. Sautet, *J. Phys. Chem. C*, 2014, **118**, 5997–6008.
32 L. V. Devi, S. Sellaiyan, S. Sankar and K. Sivaji, *Mater. Res. Express*, 2018, **5**, 024002.
33 V. V. Bannikov, I. R. Shein and A. L. Ivanovskii, *J. Supercond. Novel Magn.*, 2012, **25**, 1509–1513.
34 K. Ueda and H. Hosono, *J. Appl. Phys.*, 2002, **91**, 4768–4770.
35 R. Sa and D. Liu, *J. Mater. Res. Technol.*, 2022, **20**, 2680–2688.
36 D. Liu, L. Wu, K. Cao, H. Zeng, F. Liu and R. Sa, *Int. J. Hydrogen Energy*, 2026, **206**, 153411.
37 D. Liu, K. Cao, X. Dai and R. Sa, *Mater. Today Chem.*, 2025, **47**, 102844.
38 M. Xu, C. Qiao, K.-H. Xue, H. Tong, X. Cheng, S. Wang, C.-Z. Wang, K.-M. Ho, M. Xu and X. Miao, *J. Mater. Chem. C*, 2020, **8**, 6364–6369.
39 H. Shen, R. Yang, J. Zhou, Z. Yu, M. Lu, Y. Zheng, R. Zhang, L. Chen, W.-S. Su and S. Wang, *Phys. Chem. Chem. Phys.*, 2022, **24**, 16310–16316.
40 F. Tran, P. Blaha and K. Schwarz, *J. Phys.: Condens. Matter*, 2007, **19**, 196208.
41 S. L. Dudarev, G. A. Botton, S. Y. Savrasov, C. J. Humphreys and A. P. Sutton, *Phys. Rev. B: Condens. Matter Mater. Phys.*, 1998, **57**, 1505–1509.